Hindawi
International Journal of Corrosion
Volume 2021, Article ID 3458957, 8 pages
https://doi.org/10.1155/2021/3458957

Research Article

Heat Treatment Effect in the Corrosion Resistance of the Al-Co-Mn Alloys Immersed in 3 M KOH

J. G. Pereyra-Hernández,[1] **I. Rosales-Cadena**,[1] **R. Guardián-Tapia**,[1] **J. G. González-Rodríguez**,[1] **and R. López-Sesenes**[2]

[1]*Universidad Autónoma del Estado de Morelos, CIICAp, Av. Universidad No. 1001, Col. Chamilpa, Cuernavaca, Morelos, 62209, Mexico*
[2]*Universidad Autónoma del Estado de Morelos, FCQeI, Av. Universidad No. 1001, Col. Chamilpa, Cuernavaca, Morelos, 62209, Mexico*

Correspondence should be addressed to R. López-Sesenes; rlopez@uaem.mx

Received 31 August 2021; Accepted 8 October 2021; Published 3 November 2021

Academic Editor: Michael J. Schütze

Al-based alloys named M1, M2, M3, M4, and M5 doped with different atomic percentage (at%) of cobalt and manganese as cast and submitted at two heat treatments (600°C and 1100°C) were analyzed by using electrochemical techniques to evaluate their corrosion resistance immersed in 3 M KOH. With the heat treatments applied to the alloys, the sample M2 (65% Al, 20% Co, and 15% Mn) observed the highest corrosion resistance with R_p values of 3.0×10^2, 6.2×10^2, and $1.61 \times 10^3\ \Omega \cdot \text{cm}^2$ as cast, 600°C, and 1100°C, respectively. The latter was in agreement with the I_{corr} calculated from the polarization curves where the values decrease based on the heat treatment applied as follows: $1.60 \times 10^3 > 6.16 \times 10^2 > 3.07 \times 10^2$ mA/cm^2 for 1100, 600, and as cast, respectively. Co concentration above 20% increases the corrosion current (I_{corr}) and decreases the polarization resistance of the remain samples. The chemical analysis done with EDS and X-ray diffraction made confirmed the presence of compounds such as CoAl, Co_2Al_5, Co_2Al_9, $MnAl_4$, and $MnAl_6$.

1. Introduction

Several studies are focused on developing clean energies using new materials reducing the use of fuels from hydrocarbons. The production of electricity is one that is shifted to find new way to generate energy suitable with eco-friendly materials increasing their lifetime. One of these alternatives are the metal air batteries which in the last years are under attention due to their high energy density and capacity on load and temperature [1, 2]. Based on the latter, aluminum-based alloys as air battery doped with some metal ions had been reported by different authors with metals such as $Al^{3+,}$ Mg^{2+}, Ti^{4+}, Cr^{3+}, Zn^{2+}, Co^{3+}, Ga^{3+}, and Ti^{4+} [3–5], due mainly to their electrical and chemical properties, as well as to their low-cost acquisition compared with other metals like lithium and zinc [4]. Some authors had reported that the major problems that this kind of batteries present are their high corrosion rate and their high hydrogen evolution when in contact with the electrolyte conducing to a low anodic efficiency [6] Electrochemical techniques such as polarization curves, cyclic voltammetry, and electrochemical impedance spectroscopy had been employed to evaluate its properties with the aim to improve its physical and chemical features [7, 8]. Based on the latter, in the present research, three sets of aluminum-based alloy doped with manganese (Mn) and cobalt (Co) at different weight percentage and submitted at two heat treatments were analyzed and evaluated to modify their physical properties looking to improve their service life and offer an alternative to use as metal air battery.

2. Experimental Procedure

2.1. Materials. Table 1 shows the atomic percentages defined to synthetize the aluminum-based alloys doped with cobalt

Table 1: Atomic percentages for the Al-based alloys doped with Co-Mn as cast.

Sample	Al	Co	Mn
		At (%)	
M1	70	10	20
M2	65	20	15
M3	60	35	5
M4	58	15	27
M5	40	30	30

and manganese (M1, M2, M3, M4, and M5); each element had 99.9% purity. They were cut with a cutting machine Leco Vc-50 provided with a diamond disk. After that, they were ground with emery cloth 80, 120, 320, and 600 grade and cleaned with acetone in ultrasonic bath to eliminate rust over the metal surface to finally be weighed. For the melting process, an electromagnetic induction muffle furnace at 10^{-3} Tor of vacuum was used. The melting temperature was established at 1100°C applied around 30 min. After that, the temperature was gradually decreased until the muffle furnace was cooled while leaving the samples in the vacuum chamber.

Two heat treatments at 600°C and 1100°C were applied to the Al-based alloys with the aim to observe whether a change in the microstructure affect their corrosion resistance.

2.2. Characterization. To reveal the microstructure of the Al-based alloys as cast and with heat treatments, the samples were encapsuled into epoxy resin, ground with emery cloth 120, 220, 320, 400, 600, 800, 1000, 1500, and 2000 grade using a LECO polishing machine. Finally, based on the norm ASTM E3, alumina (Al_2O_3) at 0.05 μm of size was used as lubricant with a medium nap cloth synthetic suede as surface. After that, an etching attack was carried out using a Kroll solution with 80 ml H_2O, 10 ml HNO_3, and 6 ml HF. To observe their microstructure and determine their chemical composition, micrographs of the metal surface were recording with a scanning electron microscopy (SEM) LEO 1450 VP as well as a dispersive X ray spectroscopy method was applied to analyze the compounds in their identified phases.

2.3. Electrochemical Analysis. The corrosion behavior of the Al-based alloys as cast and with heat treatments was evaluated by using electrochemical techniques such as electrochemical impedance spectroscopy (EIS) and potentiodynamic polarization curves with a Gamry PC4 300 by Gamry Instrument as well as a Gill Potentiostat, respectively. A conventional electrochemical cell of three electrodes was used. Al-based alloy as cast and with heat treatments was used as working electrodes encapsuled in epoxy resin with an unmask area of 1 cm^2, grounding with emery paper 120, 320, 600, and 800. An electrode of Ag/AgCl was used as reference electrode, and a graphite rod was used as auxiliary electrode. The electrolyte medium was 3 M KOH at room temperature. For the EIS analysis, a frequency of 10^{-2} to 10^4 Hz with a sinusoidal amplitude of 10 mV rms was applied, recording 10 points/decade at 0 V vs. open

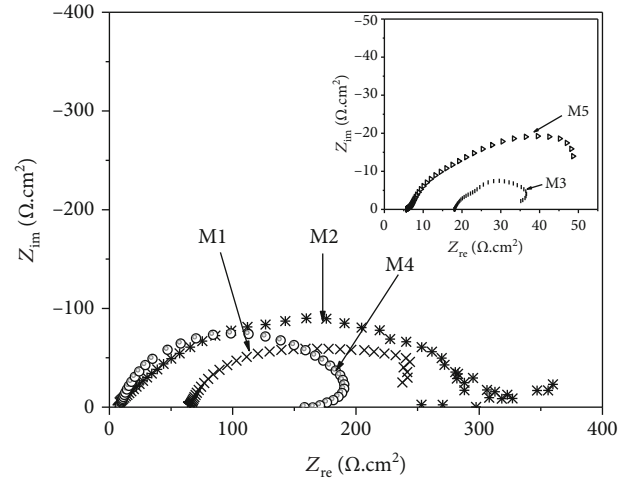

Figure 1: Nyquist plots for aluminum-based alloy doped with Mn and Co as cast, immersed in 3 M KOH.

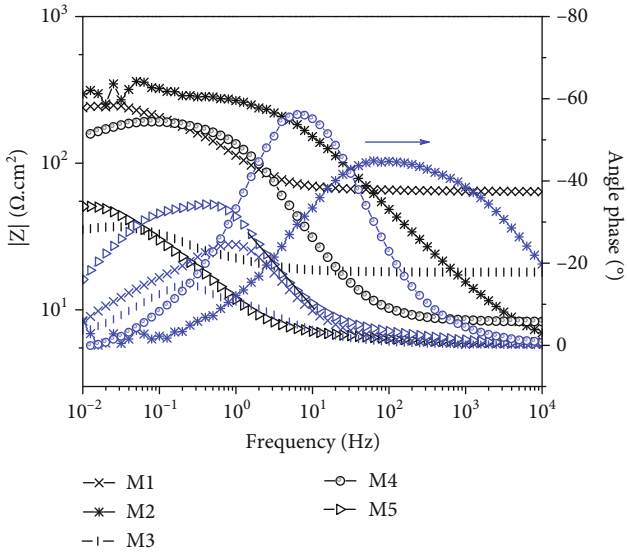

Figure 2: Modulus impedance and angle for aluminum-based alloy doped with Mn and Co as cast, immersed in 3 M KOH.

circuit potential (OCP). The potentiodynamic polarization curves were done applied a potential from -1000 to 1000 mV with a sweep rate of 60 mV/min vs. Ag/AgCl. Crosssection micrographs of the corroded samples were taken by scanning electron microscopy (SEM) LEO 1450 VP provided with an energy dispersive X-ray analyzer (EDS).

3. Result and Discussion

3.1. Electrochemical Impedance Spectroscopy (EIS). Figure 1 shows the Nyquist plot obtained from EIS analysis that was done to the aluminum-based alloys with Co and Mn as cast. From that, it is possible to observe from high to middle frequencies the formation of a capacitive loop with its center in the real axis typical of a transfer charge process from the electrolyte to the metal surface with a short

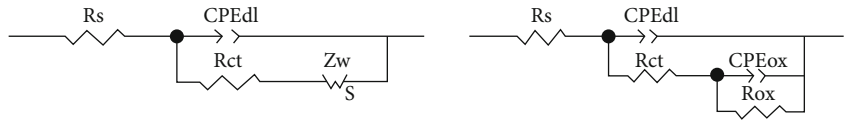

Figure 3: Equivalent circuits to fit the EIS results for the Al-based alloy doped with Mn and Co as cast and with heat treatments.

Table 2: Impedance parameters obtained through the equivalent circuit for aluminum-based alloy doped with Mn and Co as cast, immersed in 3 M KOH.

Sample	R_s (Ω·cm^2)	CPE$_{dl}$ (F·cm^2)	n_{dl}	R_{ct} (Ω·cm^2)	R_W (Ω·cm^2)	CPE$_w$ (F·cm^2)	n_w	R_p (Ω·cm^2)
M1	63.8	6.6×10^{-3}	0.7	183.5	32.2	3.4×10^{-1}	0.6	2.8×10^2
M2	4.4	4.1×10^{-4}	0.6	2.42×10^2	60.7	5.4×10^{-2}	0.5	3.0×10^2
M3	18.0	3.8×10^{-2}	0.7	16.3	5.6	9.7×10^{-1}	0.5	39.9
M4	8.2	1.2×10^{-3}	0.8	1.9×10^2				1.9×10^2
M5	5.9	6.7×10^{-2}	0.8	55.4	8.4	9.2×10^{-1}	0.5	69.7

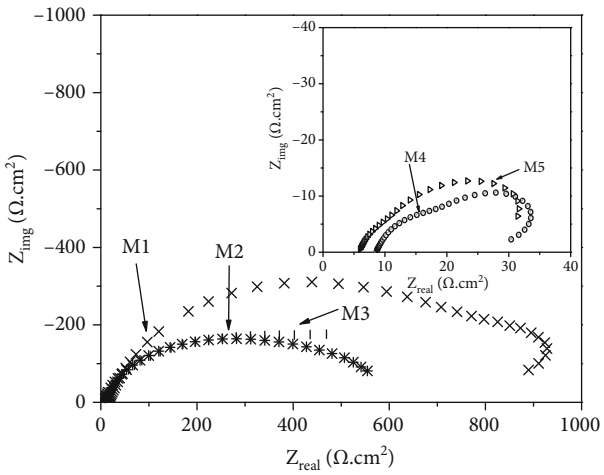

Figure 4: Nyquist plots for aluminum-based alloy doped with Mn and Co after heat treatment at 600°C immersed in 3 M KOH.

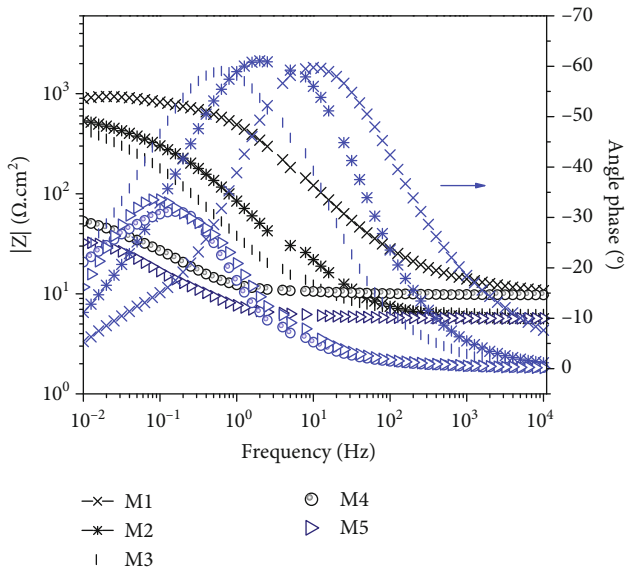

Figure 5: Modulus impedance and angle phase for aluminum-based alloy doped with Mn and Co after heat treatment at 600°C immersed in 3 M KOH.

diffusion zone except for the M4 sample. The M2 sample got the highest corrosion resistance ($3.0 \times 10^2\ \Omega \cdot \text{cm}^2$) followed by the M1 sample ($2.8 \times 10^2\ \Omega \cdot \text{cm}^2$); this can be due meanly its cobalt contained (less than 20%), helping to form a film of corrosion products which is stable in alkaline and neutral solutions [9], improving the corrosion resistance of the samples M2 and M1. However, the remaining samples (M3, M4, and M5) have a decrease in their polarization resistance (R_p) due to that they contain Co above 20%; it could be explained since the galvanic couple point of view because the Co and Mn have a potential of -0.28 and -1.63 V, respectively [10, 11], influencing the increasing or decreasing of second phases in the matrix [12, 13] which are more or less active against Al (-0.700 V/SCE) [14], generating a galvanic couple between them.

The bode-phase plots (Figure 2) show a slope change at 0.1 Hz suggesting the formation of a second time constant [15]; this corresponds with the passive film formed by the oxide products over the metal surface which is not heterogeneous based on the slope value (n) calculated which is less than 1. From high to middle frequencies, the angle phase tends to -90° for M4 and M2 samples, attributed to a not heterogonous film protective over the metal surface, meaning a not completed capacitive behavior, consistent with the charge transfer process observed in the Nyquist plots. For M1, M3, and M5, the behavior is pure resistive since its angle phase is near to 0° appearing from middle to low frequencies. At middle frequencies M1, M2, M3, and M5 shown a diffusion limited process. The equivalent circuit used to calculate the impedance parameter are showed in Figure 3, where the n parameter gets values between 0 and 1 that correspond with a heterogenous metal surface, R_{ct} is the charged transfer resistance, R_{ox} is the resistance of the corrosion products formed between the inner and outer metal-electrolyte interface, CPE$_{dl}$ is the constant phase element that correspond with the admittance Y_0 of the system for the double layer, CPE$_{ox}$ is the constant phase element for the oxide

Table 3: Impedance parameters obtained through the equivalent circuit for aluminum-based alloy doped with Mn and Co after heat treatment at 600°C immersed in 3 M KOH.

Sample	R_s ($\Omega\cdot cm^2$)	CPE_{dl} ($F\cdot cm^2$)	n_{dl}	R_{ct} ($\Omega\cdot cm^2$)	CPE_{ox} ($F\cdot cm^2$)	n_{ox}	R_{ox} ($\Omega\cdot cm^2$)	R_p ($\Omega\cdot cm^2$)
M1	9.0	2.2×10^{-4}	0.8	7.2	3.3×10^{-4}	0.8	8.91×10^{2}	9.1×10^{2}
M2	4.4	2.5×10^{-6}	0.5	1.7	1.0×10^{-3}	0.8	6.1×10^{2}	6.2×10^{2}
M3	6.4	5.5×10^{-3}	0.7	4.5×10^{2}	7.8×10^{-2}	0.9	1.25×10^{2}	5.9×10^{2}
M4	8.4	2.7×10^{-2}	0.9	4.2	4.8×10^{-1}	0.9	34.5	47.1
M5	5.8	4.5×10^{-2}	0.8	15.3	1.0×10^{-2}	0.9	20.3	41.4

film formed by the corrosion products, and Z_w is the limit diffusion process of -OH^- molecules into the metallic surface that normally is composed by a pseudoresistance (R_w) and a pseudoconstant phase element CPE_w [16]. The fitting results are listed in Table 2.

The Nyquist plots at 600°C (Figure 4) shows an increase in the polarization resistance (R_p) for M1, M2, and M3 against the samples as cast. A depressive loop semicircle that corresponds with a charge transfer system is evident again from high to middle frequencies. The diameter of a semicircle is affected by Co and Mn contained into the aluminum matrix promoting the formation of cathodic and anodic sites increasing the corrosion process over the metal surface as was explained based on the free potential of the compounds contained in the second phases.

The angle phases for all samples (Figure 5) showed a displacement in their time constant between middle and low frequencies (10^3 and 10^{-1} Hz) for the M1, M2, and M3 samples with a capacitive behavior. While, at low frequencies (<0.1 Hz), they are more resistive with values near to 0°, whereas the M4 and M5 are more resistive at high and middle frequencies and increased slightly their angle phase at low frequencies. The data were fitted, and the results are listed in Table 3 where the highest polarization resistance is for M1 with a R_p of $9.1\times10^2\,\Omega\cdot cm^2$.

When the samples are exposed to 1100°C, the Nyquist plot (Figure 6) shows only one depressive semicircle which increase or decrease based on the role played by the balance composition of the alloying employed. Only one constant phase is observed (Figure 7). The data were fitted, and the results are listed in Table 4. The highest polarization resistance (R_p) recorded was for M2 with $1.61\times10^3\,\Omega\cdot cm^2$; it is important to observe that the R_p for M2 increases with the heat treatment as follows: $1.61\times10^3 > 6.2\times10^2 > 3.0\times10^2$ for 1100, 600, and as cast, respectively, observing a positive effect of the heat treatment in the corrosion resistance of this alloy.

3.2. Polarization Curves. Polarization curves for the Al alloy doped with Co and Mn as cast, 600°C, and 1100°C are given in Figures 8–10, respectively. An active-passive behavior was observed suggesting the formation of a passive layer of corrosion products that protect the metallic surface in agreement with the impedance result. The parameters obtained from the polarization curves are showed in Table 5.

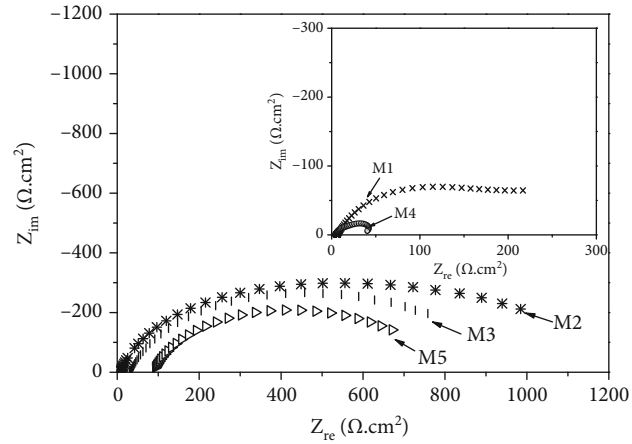

Figure 6: Nyquist plots for aluminum-based alloy doped with Mn and Co after heat treatment at 1100°C immersed in 3 M KOH.

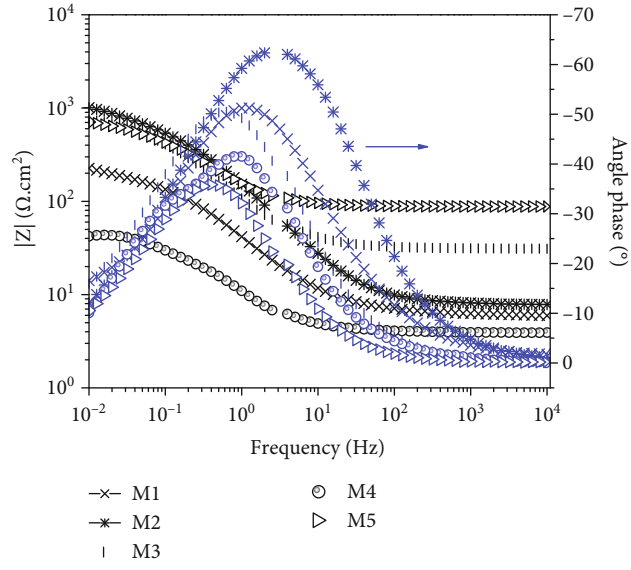

Figure 7: Modulus impedance and angle phase for aluminum-based alloy doped with Mn and Co after heat treatment at 1100°C immersed in 3 M KOH.

The current density for the samples as cast (Figure 8) does not give a significant change for M1, M2, and M3 even with the variation of Mg and Co contained in the aluminum matrix. A decrement for M4 with an I_{corr} of 1.83×10^{-5}

Table 4: Impedance parameters obtained through the equivalent circuit for aluminum-based alloy doped with Mn and Co after heat treatment at 1100°C heat treatment immersed in 3 M KOH.

Sample	R_s (Ω·cm^2)	CPE_{dl} (F·cm^2)	n_{dl}	R_{ct} (Ω·cm^2)	CPE_{ox} (F·cm^2)	n_{ox}	R_{ox} (Ω·cm^2)	R_p (Ω·cm^2)
M1	6.2	7.1×10^{-3}	0.7	2.2×10^{2}	2.7×10^{-1}	0.9	7.5×10^{1}	3.0×10^{2}
M2	8.0	9.8×10^{-6}	0.5	8.4	1.4×10^{-3}	0.8	1.6×10^{3}	1.61×10^{3}
M3	31.3	2.2×10^{-3}	0.7	6.7×10^{2}	4.5×10^{-2}	0.6	3.0×10^{2}	1.0×10^{3}
M4	3.9	3.8×10^{-2}	0.9	6.04	5.7×10^{-2}	0.9	5.0×10^{1}	5.9×10^{1}
M5	87.8	1.7×10^{-3}	0.8	4.6×10^{2}	1.1×10^{-2}	0.7	2.3×10^{2}	7.77×10^{2}

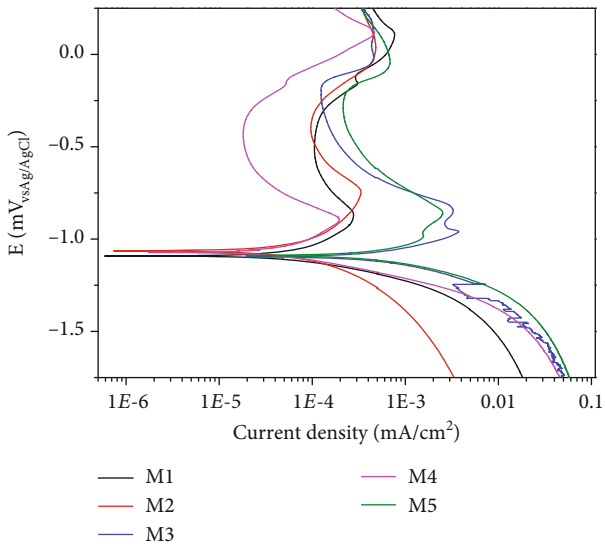

Figure 8: Polarization curves for aluminum-based alloy doped with Mn and Co as cast immersed in 3 M KOH.

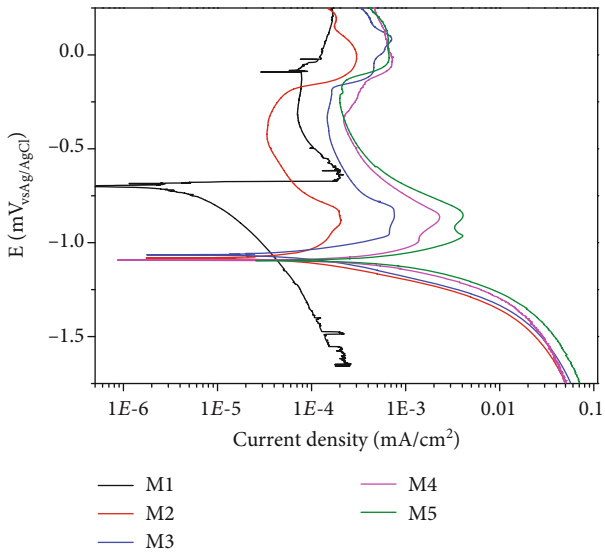

Figure 9: Polarization curves for aluminum-based alloy doped with Mn and Co after heat treatment at 600°C immersed in 3 M KOH.

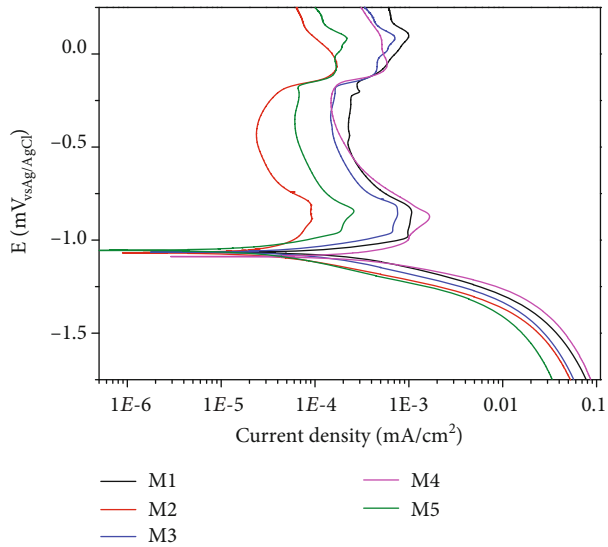

Figure 10: Polarization curves for aluminum-based alloy doped with Mn and Co after heat treatment at 1100°C immersed in 3 M KOH.

mA/cm^2 was observed with a passivation zone around -0.89 V follows by a breaking down of the passive film at -0.35 V. The highest I_{corr} was for M5 with 2.13×10^{-4} mA/cm^2. Otherwise, the cathodic branch observed an oxygen reduction process followed for a hydrogen evolution for all tests. It is important to remark that the highest I_{corr} values were recorded for M3 and M5 with a breaking down of the passive film around 0.17 V, while for remainder samples, it befell around 0.3 V.

For the samples with heat treatment at 600°C (Figure 9), the I_{corr} values tend to increase for M3, M4, and M5 with a passivation zone around 0.9 V with a pitting potential of -0.18, -0.33, and -0.15 V, respectively. M1 and M2 showed the lowest I_{corr} values as follows: M2 > M1 (3.39×10^{-5} and 6.94×10^{-5} mA/cm^2, respectively); the passive potential recorded both M2 and M1 were -0.6 and 0.8 V, with a pit potential for M1 of 0.06 V and for M2 of 0.3 V.

For the Al-based alloys with heat treatment at 1100°C (Figure 10), the highest I_{corr} values were recorded for M1, M3, and M4. All samples had a passivation zone around -0.8 V with a pitting potential near to -0.17 V. Moreover, M2 and M5 showed the lowest I_{corr} values as follows: M2 < M5 (2.33×10^{-5} and 6.16×10^{-5} mA/cm^2, respectively).

Table 5: Parameters obtained from polarization curves for aluminum-based alloy doped with Mn and Co as cast and after heat treatments at 600 and 1100°C.

	Sample				
	M1	M2	M3	M4	M5
As cast					
E_{corr} (V)	-1.09	-1.06	-1.10	-1.07	-1.09
I_{corr} (mA/cm^2)	1.06×10^{-4}	9.65×10^{-5}	1.24×10^{-4}	1.83×10^{-5}	2.13×10^{-4}
E_{pit} (V)	-0.31	-0.36	-0.17	-0.35	-0.19
I_{pit} (mA/cm^2)	1.30×10^{-4}	9.78×10^{-5}	1.28×10^{-4}	1.89×10^{-5}	2.19×10^{-4}
E_{pass} (V)	-0.86	-0.74	-0.95	-0.89	-0.85
I_{pass} (mA/cm^2)	2.75×10^{-4}	3.28×10^{-4}	3.18×10^{-3}	1.92×10^{-4}	2.51×10^{-3}
600 °C					
E_{corr} (V)	-0.70	-1.08	-1.07	-1.09	-1.10
I_{corr} (mA/cm^2)	6.94×10^{-5}	3.39×10^{-5}	1.49×10^{-4}	2.16×10^{-4}	1.97×10^{-4}
E_{pit} (V)	-0.06	-0.34	-0.18	-0.33	-0.15
I_{pit} (mA/cm^2)	7.48×10^{-5}	3.39×10^{-5}	1.49×10^{-4}	2.19×10^{-4}	2.00×10^{-4}
E_{pass} (V)	-0.63	-0.82	-0.95	-0.85	-0.96
I_{pass} (mA/cm^2)	1.97×10^{-4}	2.06×10^{-4}	7.58×10^{-4}	2.29×10^{-3}	4.16×10^{-3}
1100°C					
E_{corr} (V)	-1.07	-1.07	-1.20	-1.09	-1.05
I_{corr} (mA/cm^2)	2.19×10^{-4}	2.33×10^{-5}	1.44×10^{-4}	1.53×10^{-4}	6.16×10^{-5}
E_{pit} (V)	-0.15	-0.17	-0.24	-0.23	-0.17
I_{pit} (mA/cm^2)	2.26×10^{-4}	2.44×10^{-5}	1.46×10^{-4}	1.51×10^{-4}	6.63×10^{-5}
E_{pass} (V)	-0.84	-0.80	-0.96	-0.86	-0.84
I_{pass} (mA/cm^2)	1.08×10^{-3}	9.35×10^{-5}	7.70×10^{-4}	1.65×10^{-3}	2.55×10^{-4}

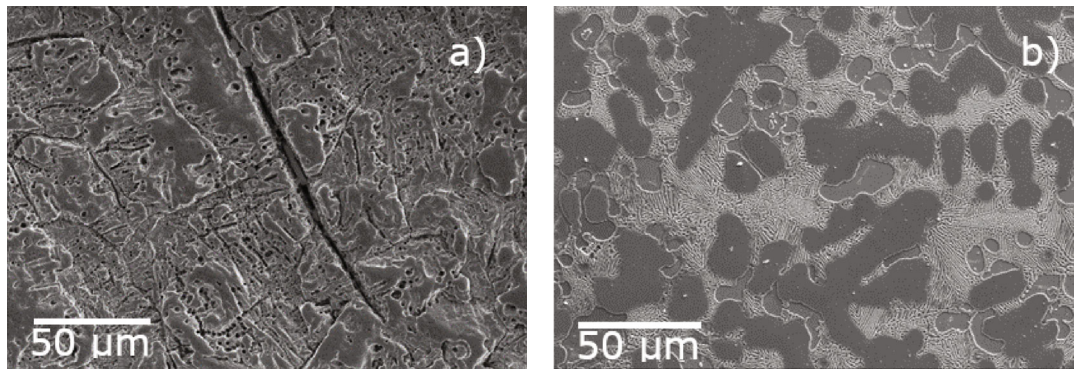

(a) (b)

Figure 11: Micrographs recorded for the M1 (a) and M4 (b) aluminum-based alloy doped with Co and Mn.

Figure 11 shows an example of the micrographs for M1 and M4 aluminum-based alloy enriched with -Mn and Co, where is possible observe a shift in the microstructure morphology based on its Al contain noticing the formation of two phases. For M1, phase 1 consists a dendritic form that has Mn and Al in its composition (50 and 35%wt.) forming meanly $MnAl_4$ and $MnAl_6$ compounds with low Co contain, whereas phase 2 corresponds with the Al matrix at a 50%wt. with containing low Mn and Co (25%wt., to each one), forming CoAl, Co_2Al_5, and $MnAl_6$ (Figure 12). The latter is confirmed with the X-ray patterns done for the Al alloys doped with Co and Mn at different concentration as cast (Figure 13) where were found the compounds mentioned in both phases 1 and 2.

After the alloys were exposed to 3 M NaOH, a crosssection recorded by SEM (Figure 14) confirms the presence of a layer of corrosion products with diffusion of O^- and H^+ ions with a deep around 540 and 200 μm for M1 and M4

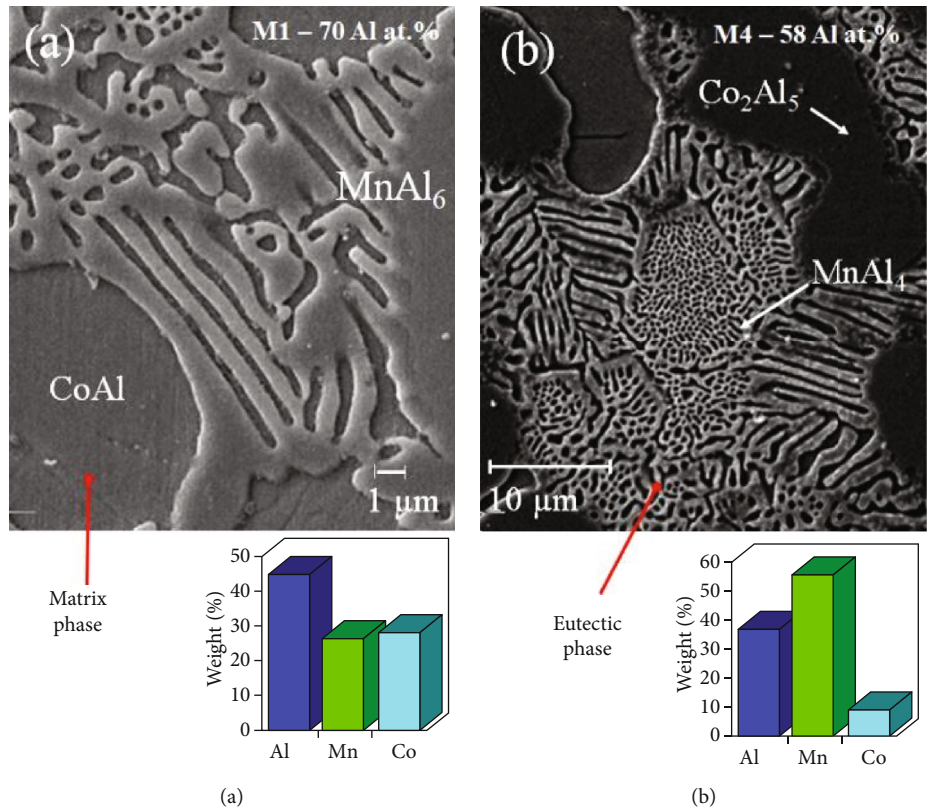

(a) (b)

Figure 12: SEM and EDS analysis in the matrix and second phase for the M1 and M4 samples as cast.

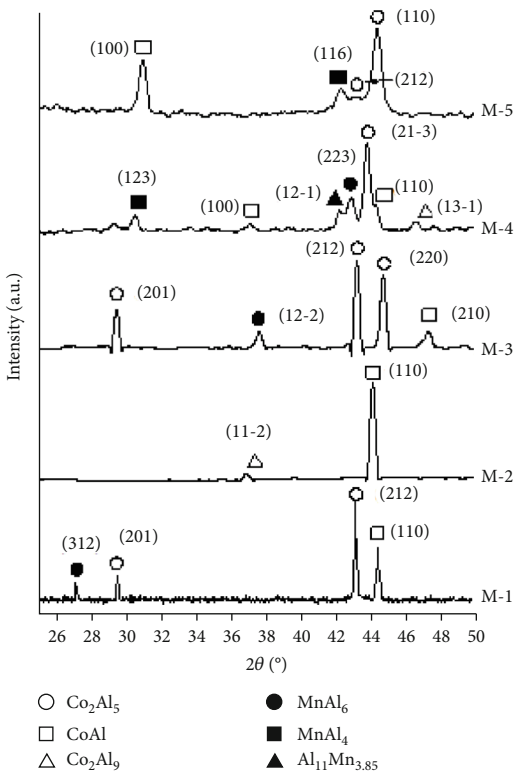

Figure 13: X-ray diffraction analysis for the Aluminum-based alloy M1, M2, M3, M4 and M5 doped with Co and Mn as cast.

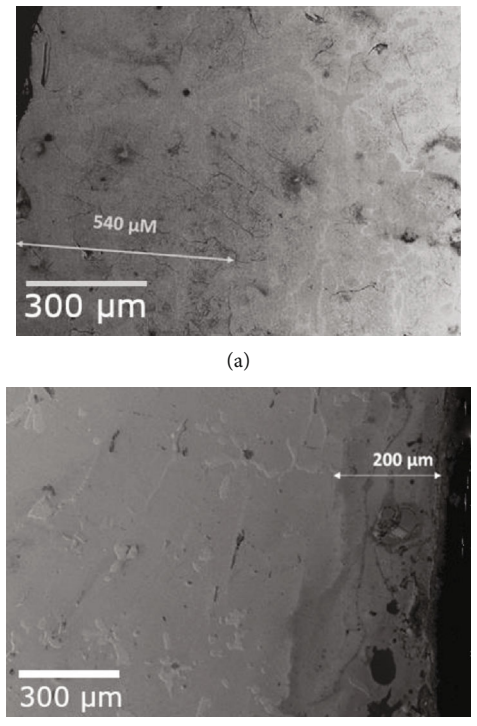

Figure 14: Crosssection of M1 (a) and M4 (b) samples after immersed in 3 M KOH.

alloys, respectively. These observed a generalized corrosion mainly that Al alloys have the trend to form a protective layer of corrosion products normally Al_2O, MnO, and Mn_5O_8 explaining the increment in the corrosion resistance that was appreciated in the electrochemical analysis.

4. Conclusions

Based on the analysis carried out, we can conclude that the M2 aluminum-based alloy enriched with Co and Mn is a good candidate to be used as air battery material since its resistance increased when it was submitted to heat treatments. To the remaining alloys, it should be taken in account that the cobalt concentration above 20% wt. affects the corrosion resistance of the alloys even with heat treatments; this behavior was attributed that they present two phases in their microstructure where the first phase consists in a dendritic form that have in its composition Mn and Al (50 and 35%wt.), whereas the second phase corresponds with the Al matrix with low Mn and Co appearing microgalvanic cells with different potential over the metal surface promoting the corrosion processes.

Data Availability

The data and all analyses used to support the findings of this study are included within the article.

Conflicts of Interest

The authors declare that they have no conflicts of interest.

References

[1] Z.-L. Wang, D. Xu, J.-J. Xu, and X.-B. Zhang, "Oxygen electrocatalysts in metal–air batteries: from aqueous to nonaqueous electrolytes," *Chemical Society Reviews*, vol. 43, no. 22, pp. 7746–7786, 2014.

[2] M. A. Rahman, X. Wang, and C. Wen, "High energy density metal-air batteries: a review," *Journal of the Electrochemical Society*, vol. 160, no. 10, pp. A1759–A1771, 2013.

[3] M. Iftekhar, N. E. Drewett, A. R. Armstrong et al., "Characterization of aluminum doped lithium-manganese rich composites for higher rate lithium-ion cathodes," *Journal of the Electrochemical Society*, vol. 161, no. 14, pp. A2109–A2116, 2014.

[4] Z. He, Z. Wang, H. Chen et al., "Electrochemical performance of zirconium doped lithium rich layered $Li_{1.2}Mn_{0.54}Ni_{0.13}Co_{0.13}O_2$ oxide with porous hollow structure," *Journal of Power Sources*, vol. 299, pp. 334–341, 2015.

[5] V. Sethuprakhash and W. J. Basirun, "Structural and electrochemical investigation of LiNi0.8Co0.2 – xMxO2 (M = Al, Al +Mg, Al+Mg+Fe) synthesized by solid-state method," *Ionics*, vol. 14, pp. 501–507, 2008.

[6] Y. Tang, L. Lu, H. Roesky, L. Wang, and B. Huang, "The effect of zinc on the aluminum anode of the aluminum-air battery," *Journal of Power Sources*, vol. 138, no. 1-2, pp. 313–318, 2004.

[7] P. Hartmann, D. Grübl, H. Sommer, J. Janek, W. G. Bessler, and P. Adelhelm, "Pressure dynamics in metal–oxygen (metal–air) batteries: a case study on sodium superoxide cells," *The Journal of Physical Chemistry C*, vol. 118, no. 3, pp. 1461–1471, 2014.

[8] J. Adams, M. Karulkar, and V. Anandan, "Evaluation and electrochemical analyses of cathodes for lithium-air batteries," *Journal of Power Sources*, vol. 239, pp. 132–143, 2013.

[9] M. Metikoš-Huković and R. Babić, "Passivation and corrosion behaviours of cobalt and cobalt-chromium-molybdenum alloy," *Corrosion Science*, vol. 49, no. 9, pp. 3570–3579, 2007.

[10] R.-c. Zeng, J. Zhang, W.-j. Huang et al., "Review of studies on corrosion of magnesium alloys," *Transactions of Nonferrous Metals Society of China*, vol. 16, pp. s763–s771, 2006.

[11] X. Li, G. Pan, C. Wang, X. Guo, P. He, and Y. Li, "Effect of chelating agent on reducing galvanic corrosion between cobalt and copper in alkaline slurry," *ECS Journal of Solid State Science and Technology*, vol. 5, no. 9, pp. P540–P545, 2016.

[12] L. Jiang, F. Xu, Z. Xu et al., "Biodegradation of AZ31 and WE43 magnesium alloys in simulatedbBody fluid," *International Journal of Electrochemical Science*, 2015.

[13] S. Valdez, "Effect of silver composition on electrochemical degradation of alzn alloy," *International Journal of Electrochemical Science*, 2013.

[14] K. B. Deshpande, "Validated numerical modelling of galvanic corrosion for couples: magnesium alloy (AE44)-mild steel and AE44-aluminium alloy (AA6063) in brine solution," *Corrosion Science*, vol. 52, no. 10, pp. 3514–3522, 2010.

[15] Y. B. Amor, E. M. M. Sutter, H. Takenouti, M. E. Orazem, and B. Tribollet, "Interpretation of electrochemical impedance for corrosion of a coated silver film in terms of a pore-in-pore model," *Journal of the Electrochemical Society*, vol. 161, no. 14, pp. C573–C579, 2014.

[16] S. H. Ahn, Y. S. Choi, J. G. Kim, and J. G. Han, "A study on corrosion resistance characteristics of PVD Cr-N coated steels by electrochemical method," *Surface and Coatings Technology*, vol. 150, no. 2-3, pp. 319–326, 2002.